# Targeted β-phase formation in poly(fluorene)-ureasil grafted organic-inorganic hybrids

*Ilaria Meazzini[§], Jonathan M. Behrendt[‡], Michael L. Turner[‡] and Rachel C. Evans*[,§†]*

[§]School of Chemistry and CRANN, Trinity College Dublin, The University of Dublin, Dublin 2, Ireland.

[‡]School of Chemistry, University of Manchester, Oxford Road, Manchester, M13 9PL, United Kingdom.

KEYWORDS. Conjugated polymers, hybrid materials, optically active materials, photoluminescence.

ABSTRACT. The development of synthetic strategies to control the molecular organization (and inherently linked optoelectronic properties) of poly(fluorene)s is critical for the development of efficient light-emitting devices. Here, we report a facile route using sol-gel chemistry to promote the formation of the β-phase through the covalent-grafting of poly[(9,9-dioctylfluorene)-*co*-(9,9-bis(8-hydroxyoctyl)fluorene)] (PFO-OH) to poly(oxyalkylene)/siloxane hybrids known as *ureasils*, due to the urea linkages binding the organic and inorganic components. Although grafting occurs within the siliceous domains, the degree of branching of the organic backbone determines the packing of the PFO-OH chains within the ureasil framework. Moreover, photoluminescence studies indicate that physical

confinement also plays a key role in promoting the evolution of the β-phase of PFO-OH as the sol-gel transition proceeds. Spectroscopic and structural analyses reveal that di-branched ureasils promote linear packing of the PFO-OH chains, whilst tri-branched ureasils exhibit a more open, distorted structure, that restricts the packing efficacy and reduces the number of covalent anchorages. These results indicate that the organic-inorganic hybrid structure induces distinct levels of β-phase formation and that covalent-grafting is a versatile approach to design novel poly(fluorene) hybrid materials with tailored optical properties.

## INTRODUCTION

The intense blue emission and high photoluminescence quantum yields of polyfluorenes (PFs) have led to their widespread deployment as active components in polymer light-emitting diodes[1-5] and sensors and diagnostics.[6-11] Conjugated polymers derive their unique optoelectronic properties from the delocalized electronic structure of the polymer backbone, which is intrinsically linked to the conformation of the polymer chains. PFs in particular are known to exhibit different intra- and intermolecular conformations in the solid, liquid and gel states.[12-14] The rich phase behavior of poly(9,9-dioctylfluorene) (PFO), an archetypical member of this materials class, has been well-studied. PFO is polymorphic, with the most prevalent states including an amorphous α-phase,[15] a weakly-ordered planar β-phase[16] or the more recently discovered monoclinic γ-phase,[17] which is intermediate between the two. These states do not represent phases in the true thermodynamic sense (*i.e.* they do not obey Gibbs' phase rule), but instead represent the interplay between the conformation of the polymer backbone and various inter- and intra-molecular interactions (π-π stacking, van der Waals forces and hydrogen bonding) occurring between individual polymer backbones and side chains, with each phase exhibiting a unique optical fingerprint.[4, 18] The β-phase is not commonly encountered in other π-conjugated macromolecules and its formation has been linked to enhanced optoelectronic properties, including improved charge carrier mobility, efficient amplified spontaneous emission and low lasing threshold limit.[19-20] However, the β-phase content is always relatively low and never fully dominates the material and as such there is significant interest in its targeted formation in both pure and hybrid PF-based materials. The β-phase is most commonly observed in polymer thin films that have been subjected to specific thermal or vapor treatment,[21-23] have been cast from a poor solvent,[24] or have been sprayed as a composite film.[25] β-phase formation has also been demonstrated in pure supramolecular gels prepared from PFO in apolar organic solvents[26] and through its confinement in a silica-based

ionogel.[27] The co-condensation of siloxane-functionalized poly(fluorene)s with an alkoxysilane monomer has also been reported to form organic-inorganic hybrid nanoparticles in which the percentage of β-phase present is controlled by the amount of alkoxysilane used.[28]

Inspired by these examples, we postulated that targeted formation of the β-phase could potentially be achieved through the covalent-grafting of a functionalized-PF to a targeted host material, which, if judiciously selected, could additionally impart thermal and photostability.[29-31] The ideal host material should also be chemically compatible with the PF, thus eliminating any potential phase separation. Moreover, the optoelectronic properties of the PF grafted onto it, should be maintained, and preferably enhanced upon incorporation. A family of covalently-linked (Class II) organic-inorganic hybrid materials known as ureasils appeared to perfectly match these host requirements. Ureasils are comprised of a siliceous skeleton that is chemically-grafted to poly(ethylene oxide) (PEO)/poly(propylene oxide) (PPO) chains through urea [NHC(=O)NH] cross-linkages, the number of which depend on the degree of branching in the organic polymer precursor (Figure 1).[32-33] Ureasils are inherently photoluminescent due to radiative recombination at localized sites in both the siliceous and urea-centered domains and have been employed as active hosts for a variety of dopants including lanthanide ions/complexes,[34-37] molecular dyes,[38] and conjugated polymers.[30, 39] Recently, we have shown that the incorporation of PF-conjugated polyelectrolytes within a di-ureasil matrix results in a dramatic increase in the photoluminescence quantum yield, due to a synergistic electronic interaction between the di-ureasil host and the conjugated polymer.[30] Moreover, the introduction of red-orange emissive poly(thiophene)s or poly(phenylene)s into the di-ureasil led to tunable white-light emission.[39] However, in both examples the conjugated polymers are physically immobilized in the di-ureasil matrix and there is no formal chemical bonding interaction.

Here, we report a novel strategy to promote the formation of the β-phase through the covalent-grafting of a hydroxyl-functionalized poly[(9,9-dioctyfluorene)-*co*-(9,9-bis(8-hydroxyoctyl)fluorene)] (PFO-OH) onto the siliceous backbone of di- or tri-podal ureasil frameworks. The organic-inorganic hybrid host provides excellent chemical compatibility for the conjugated polymer and results in a homogeneous distribution of the PFO throughout the entire material, unlike that observed for purely inorganic matrices.[19, 27] Physical confinement of the PFO within the ureasil framework promotes β-phase formation, the extent of which may be tuned by varying the PFO concentration and the degree of branching of the organic backbone of the ureasil precursor. The % contribution of β-phase formed is quantified and correlated with the optical properties of the resultant hybrid material. The results highlight how chemical-grafting approaches can be used to manipulate the conformation of conjugated polymers within a host matrix, delivering tunable optical properties.

## EXPERIMENTAL SECTION

**Materials.** Poly[(9,9-dioctylfluorene)-*co*-(9,9-bis(8-hydroxyoctyl)fluorene)] (PFO-OH) with a number-averaged molecular weight $M_n$ = 15,500 g mol$^{-1}$ was prepared following a procedure previously reported in literature.[28] Poly(propylene glycol)-*block*-poly(ethylene glycol)-*block*-poly(propylene glycol)-*bis*-(2-aminopropylether) (Jeffamine ED-600), potassium bromide (KBr) (spectroscopic grade), 3-isocyanatopropyltriethoxycyanate (ICPTES) (95.0%), tetrahydrofuran (THF) (HPLC grade), ethanol (99.0%), deuterated chloroform ($CDCl_3$) (99.8%) and hydrochloric acid (HCl) (37%) were purchased from Sigma and used as received. Trimethylolpropane *tris*[poly(propylene glycol), amine-terminated] ether (Jeffamine T-403) was obtained from Huntsman.

**Synthesis**. Samples were synthesized using a method previously reported in literature,[40-41] and are designated as DU-PF-*x* and TU-PF-*x* for di-ureasils and tri-ureasils respectively, where *x* represents the concentration of in wt% of PFO-OH in the final hybrid. For undoped ureasils,

each Jeffamine precursor (1.76 mmol) was dissolved in THF (5 mL) and refluxed with ICPTES at 70 °C for 12 hr (molar ratios: 1 : 2 and 1 : 3 for Jeffamine ED-600 : ICPTES and Jeffamine T-403 : ICPTES, respectively). Each solution was subsequently cooled to room temperature (RT), before adding EtOH, HCl (0.5 M) and $H_2O$ to initiate the acid-catalyzed hydrolysis and condensation reaction, in the molar ratio of ICPTES : EtOH : HCl : $H_2O$ is equal to 176 : 350 : 1 : 265. Each solution was stirred for 2 min between each addition, before casting into a polypropylene mould and covering with Parafilm M®. After 2 days, 5 holes were pierced in the Parafilm M® to allow the slow evaporation of THF for a further 72 hr. The drying process was completed when samples were uncovered and placed in an oven at 40 °C for 48 hr. A similar approach was followed for the synthesis of PF-doped ureasils, where a fixed volume (0.193-2.081 mL) of a stock solution of PFO-OH in THF (1 mg $mL^{-1}$) was first added to ICPTES (3.52 mmol for DU-PF, 5.28 mmol for TU-PF) in THF (2.5 mL) and stirred at RT for 4 hr. The corresponding Jeffamine (1.76 mmol) and additional THF (for each sample enough to obtain a final volume of THF equal to 5.0 mL) were then added and the solution was refluxed at 70 °C for 12 hr. The volume of the PFO-OH stock solution varied to yield a final concentration of either 0.01, 0.05 or 0.10 wt% of PFO-OH in the dry monolith. The molar ratios of the gelation reagents used in the second step and the ageing process were the same as those used for the preparation of the undoped monoliths.

**Characterization.** *Nuclear Magnetic Resonance (NMR) Spectroscopy*. For solution measurements, $^{1}H$ NMR spectra were recorded on a Bruker DPX 400 spectrometer (400 MHz) on samples dissolved in $CDCl_3$. Solid-state $^{29}Si$ and $^{13}C$ cross-polarized (CP) and directly-excited (DE) magic angle spinning (MAS) NMR measurements (for DU-PF-0, TU-PF-0, DU-PF-0.05 and TU-PF-0.05) were performed at ambient temperature on a Varian VNMRS instrument operating at 79.44 MHz for $^{29}Si$ and 100.56 MHz for $^{13}C$. Spectra were recorded against an external tetramethyl silane (TMS) standard with MAS of 6000 Hz. Additional $^{29}Si$

and $^{13}C$ CP and DE NMR measurements (DU-PF-0.01, TU-PF-0.01, DU-PF-0.1 and TU-PF-0.1) were performed at 20 °C on an Agilent 800 Hz DD2 spectrometer operating at 158.9 MHz for $^{29}Si$ and 201.1 MHz for $^{13}C$. Spectra were recorded against an external TMS standard with a MAS rate of 4200 Hz.

*Fourier Transform Infrared (FTIR) spectroscopy*. FTIR spectra were measured on a Perkin-Elmer spectrum 100 FTIR spectrometer at room temperature and collected over a range of 4000-650 $cm^{-1}$ with a resolution of 4 $cm^{-1}$. Samples (2 mg) were finely ground, mixed with potassium bromide (175 mg) and pressed into pellets. To evaluate the contributions to the Amide I band, spectral deconvo lution using Gaussian band fitting was carried out using OriginPro 8.5 (Microcal) in the region of 1600–1800 $cm^{-1}$.

*Thermogravimetric analysis (TGA)*. TGA was performed using a Perkin Elmer Pyris TGA thermogravimetric analyser in an air atmosphere between 30 to 900 °C with a heating rate of 10 °C $min^{-1}$ using *ca*. 2 mg of sample placed in a ceramic crucible.

*Powder X-ray diffraction (PXRD)*. PXRD measurements were performed on a Bruker D2 Phaser diffractometer. The samples were exposed to the Cu Kα radiation ($\lambda$ = 1.54 Å) at RT. The investigated $2\theta$ range is 5 to 70°.

*UV/Vis absorption spectroscopy*. UV/Vis absorption spectra were recorded at RT in a Perkin Elmer Lambda 1050 UV/Vis spectrometer (slit width 2 nm). The absorbance of solutions at the excitation wavelength was < 0.1.

*Photoluminescence measurements*. Steady-state photoluminescence (PL) spectroscopy was carried at room temperature (RT) on a Fluorolog-3 spectrophotometer (Horiba Jobin Yvon), with emission and excitation slits of 1 nm. Emission and excitation spectra were corrected for the wavelength response of the system and the intensity of the lamp profile over the excitation range, respectively, using correction factors supplied by the manufacturer. PL quantum yield measurements were performed using an F-3018 integrating sphere mounted into a FluoroMax-

4p spectrophotometer (Horibama Jobin Yvon). The values reported are the mean of three repeat measurements. The method is accurate within 10%. Spectral deconvolution of the excitation spectra using Gaussian fitting was performed using OriginPro 8.5 (Microcal).

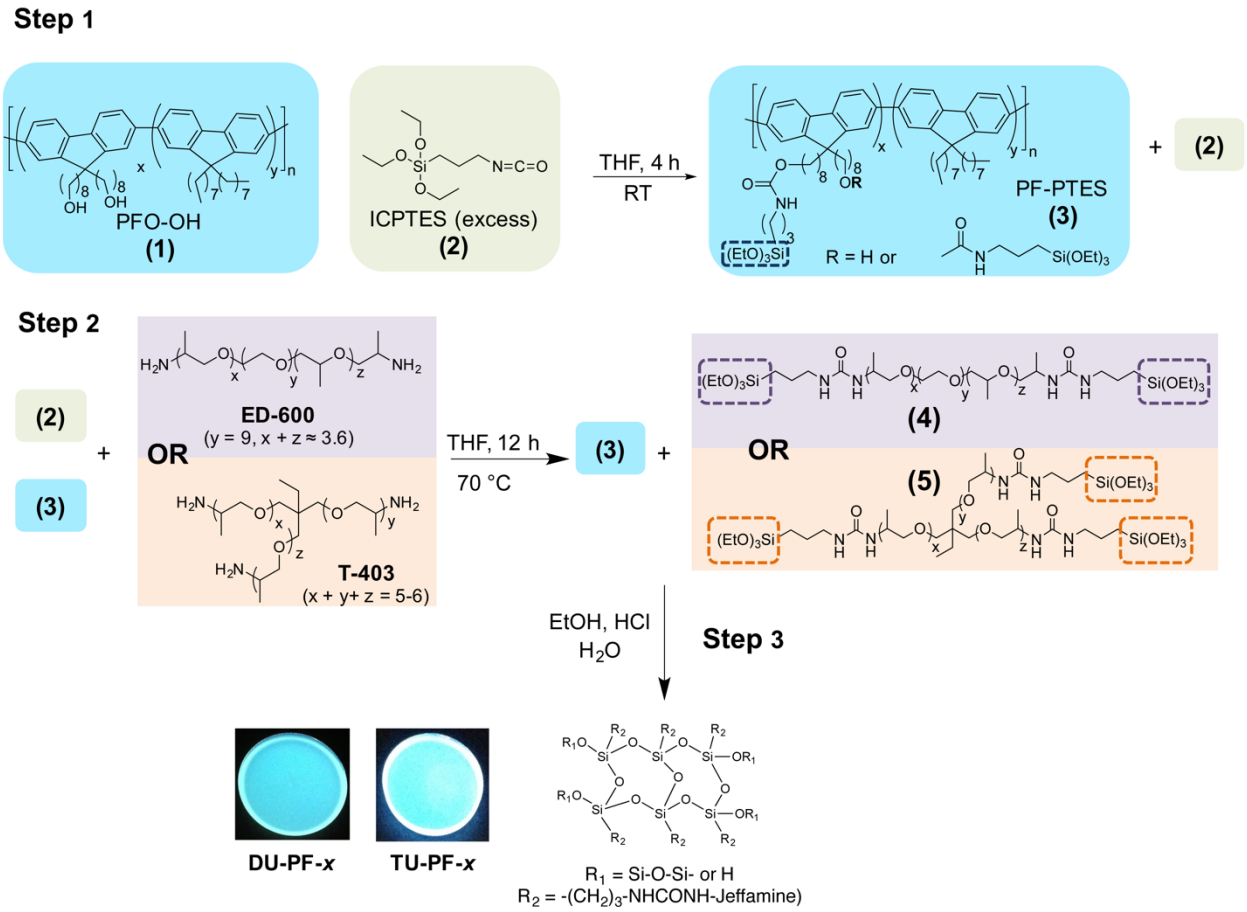


**Figure 1.** Synthetic route for the preparation of DU-PF-x and TU-PF-x.

## RESULTS AND DISCUSSION

### Synthesis of PF-grafted di- and tri-ureasils.

The synthesis of PF-grafted di- and tri-ureasils requires three distinct steps, as illustrated in Figure 1. In the first step PFO-OH (**1**) is reacted with excess 3-isocyanatopropyltriethoxysilane (**2**, ICPTES) to introduce triethoxysilyl groups onto the side-chains of the intermediate, PF-PTES (**3**). The appearance of a new signal at 4.35 ppm in the $^{1}$H NMR spectrum confirmed the formation of a carbamide bond between **1** and **2** (Figure 2).[28] However, the continued presence of the hydroxyl signal (3.61 ppm) indicates that functional loading of triethoxysilane does not

reach completion. TGA revealed that pure PFO-OH undergoes a single decomposition event initiated at *ca*. 410 °C (Figure S1). In contrast, the intermediate **PF-PTES** exhibits two thermal decomposition events, at onset temperatures of *ca*. 227 °C and *ca*. 410 °C, respectively. The first step is attributed to the loss of side chains attached to the polymer backbone, while the second is associated with decomposition of the conjugated polymer backbone. The presence of a distinct decomposition event associated with the polymer side-chains supports modification of their chemical structure compared to PFO-OH. Moreover, the low onset temperature is consistent with the degradation temperature observed for the ICPTES precursor (*ca*. 134 °C). In the second step, either Jeffamine ED-600 or Jeffamine T-403 is added to the mixture and reacts with the remaining ICPTES (present in either two or three molar equivalents excess, respectively), ensuring that all amine groups on the polyetheramine are functionalized to yield the corresponding intermediates, di-ureapropyltriethoxysilane (d-UPTES) (**4**) or tri-ureapropyltriethoxysilane (t-UPTES) (**5**).[32, 40] The reaction progress was confirmed by FTIR spectroscopy (Figure S2, Supporting Information), which revealed the disappearance of the strong vibrational peak corresponding to asymmetric stretching of the isocyanate moieties of ICPTES (2265 $cm^{-1}$), and the concomitant appearance of new vibrational bands corresponding to hydrogen bonded N-H groups (3340 $cm^{-1}$), the C=O stretch of a secondary amide (1635 $cm^{-1}$), and a bending mode of the N-H moieties (1561 $cm^{-1}$).[32, 42] In the final step, the triethoxysilyl groups on PF-PTES and d-UPTES or t-UPTES are cross-linked under acid-catalyzed sol-gel conditions to yield the final organic-inorganic ureasil hybrid as a free-standing monolith. The concentration of PFO-OH was varied to obtain a series of PF-grafted di- and tri-ureasils containing different conjugated polymer loadings (wt. %). The samples are designated as DU-PF-*x* and TU-PF-*x*, for di- and tri-ureasils, respectively, where *x* represents the final concentration (in wt. %) of PFO-OH incorporated.

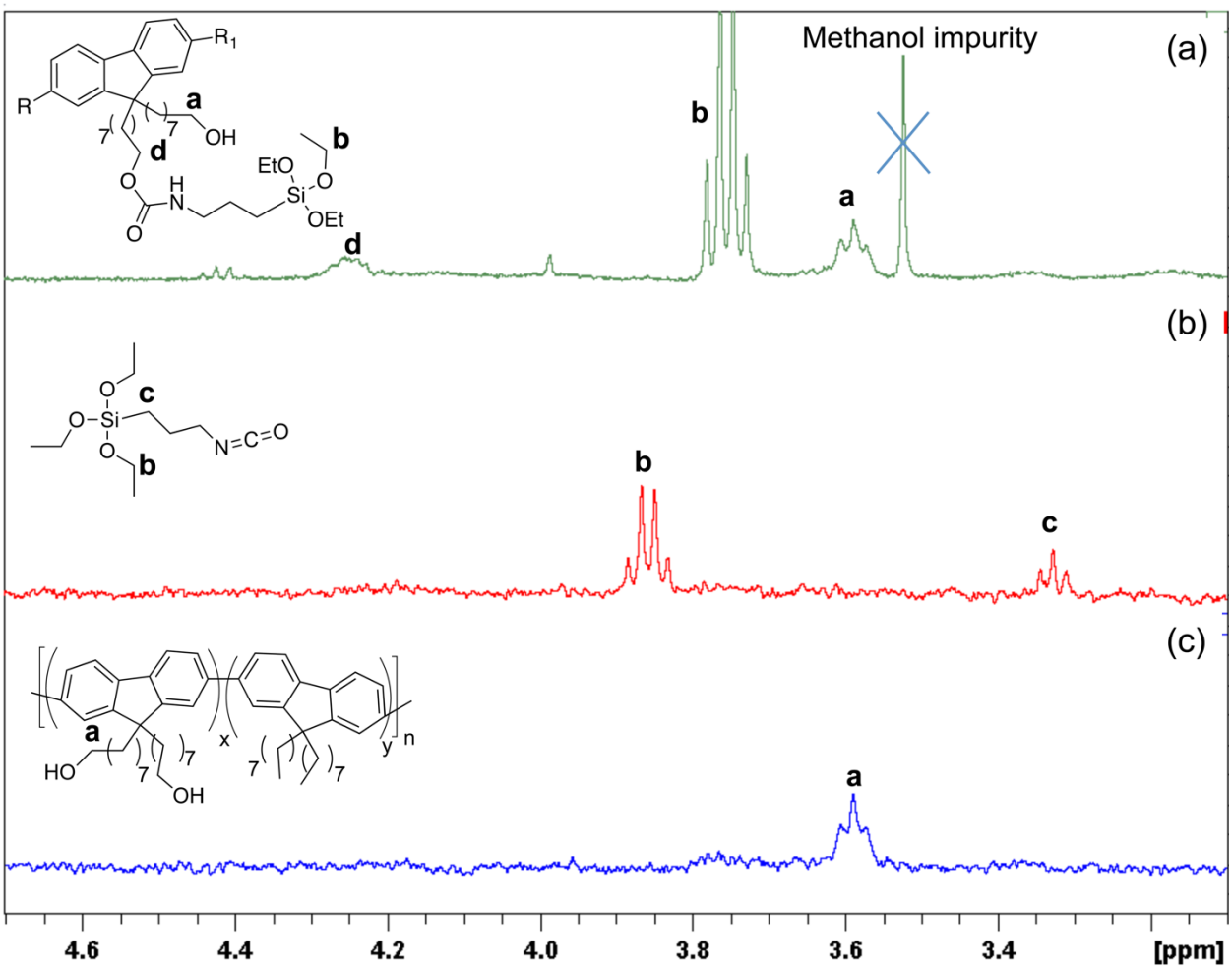


**Figure 2**. $^{1}$H NMR spectra (400 MHz, $CDCl_3$) of (a) PF-PTES (**3**), (b) ICPTES (**2**) and (c) PFO-OH (**1**).

**Structural characterization of PF-grafted di- and tri-ureasils.**

For ureasil-type materials, FTIR spectroscopy can provide valuable information about the effect of dopants/co-substituents on the final hybrid structure.[32, 41, 43] Analysis of the Amide I region (1600-1800 $cm^{-1}$) in particular can deliver direct insight into the degree and specificity of hydrogen-bonding interactions associated with C=O stretching frequencies in different local environments. Figure 3 (and Figure S3) present the results of Gaussian deconvolution of the Amide I region of DU-PF-*x* and TU-PF-*x* samples and the corresponding hydrogen-bonding interactions are shown. The peak frequencies and relative areas obtained from the Gaussian fits are reported in Table S1 of the Supporting Information. For the DU-PF-*x* series, three peaks

centered at ~1710 $cm^{-1}$ (Peak 3), ~1660 $cm^{-1}$ (Peak 2) and 1635 $cm^{-1}$ (Peak 1) are identified. These bands correspond to carbonyl stretching frequencies located within disordered hydrogen-bonded polyether-urea associations of increasing strength (Peak 3 and Peak 2, respectively) and self-organized, hydrogen-bonded urea–urea interactions (Peak 1). At low PF concentrations, a fourth peak at ~1775 $cm^{-1}$ is also observed, suggesting that carbonyl groups free of hydrogen-bonding are also present.[36] However, as the PF concentration is increased, this peak disappears and ordered urea-urea interactions (Peak 1) become more important, suggesting a slight increase in the packing density of the co-condensed PF-PTES-d-UPTES network, accompanied by a re-arrangement of the urea/polyether chain interactions, as illustrated by the simultaneous increase and decrease in the intensities of Peak 3 and Peak 2, respectively. In contrast, for the TU-PF-*x* series, Gaussian deconvolution of the Amide I region reveals the presence of peaks 1-4 at all concentrations, except 0.01 wt.%. We attribute these differences to the degree of branching of the individual Jeffamine polyetheramine precursors. We propose that the linear branching of Jeffamine ED-600 induces a more ordered and compact conformation in the DU-PF-*x* series, in which the grafted PF-chains occupy linear domains within the hybrid structure. These domains increase in size with the PF wt.%, and tend to isolate the di-ureasil backbones, favoring the formation of disordered interactions between polyether chains and urea moieties. In contrast, no specific trend is observed for the TU-PF-*x* series with increasing concentration of PFO-OH. We suggest that in this case, the PF chains can be accommodated without bringing major structural changes to the hydrogen-bonded array of the tri-ureasil.

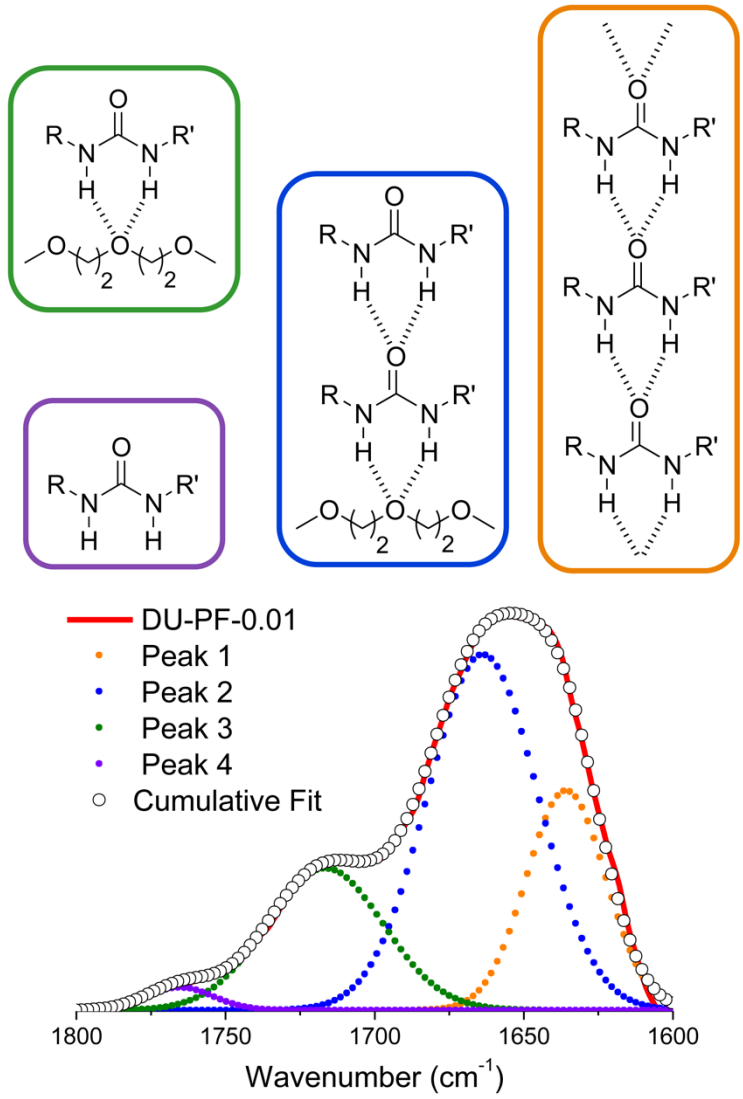


**Figure 3.** FTIR spectrum and Gaussian curve-fits of the Amide I region of DU-PF-0.01 and schematic representation of the corresponding hydrogen-bonding associations in ureasil hybrids. R and R′ represent the inorganic and organic portion of the hybrid structure.

For both DU-PF-*x* and TU-PF-*x* samples, $^{13}$C CP-MAS NMR spectroscopy confirmed the reaction of the organic precursors, with the characteristic peak corresponding to urea moieties centered at *ca*.160 ppm observed (Figure S4 and Table S2). $^{29}$Si MAS-NMR was used to probe the degree of condensation of the siliceous network in the DU-PF-*x* and TU-PF-*x* series (Figure

4). Each sample presents the characteristic signals of $T_1$ ($R'Si(OSi)(OR)_2$, ~50 ppm), $T_2$ ($R'Si(OSi)_2(OR)$, ~58 ppm) and $T_3$ ($R'Si(OSi)_3$, ~67 ppm) groups, respectively. Peak centers, relative areas and the calculated degrees of condensation, *c*,[44] are reported in Table S3 in the Supporting Information. Comparing first the pristine DU-PF-0 and TU-PF-0 samples, it is apparent that the $T_1$ signal for TU-PF-0 provides a much greater (~5x) contribution to the spectrum. This provides further indication that the TU-network is less condensed than the corresponding DU-system. Upon grafting of the PF to the material, the silica network becomes increasingly more condensed (*c*~80-84 %) for the DU-PF-*x* series, as revealed by the increased contribution from the $T_3$ signal, which is consistent with the conclusions drawn from the FTIR spectra. The corresponding degree of condensation determined for the TU-PF-*x* series is notably lower by comparison (*c*~69-79%), although no specific trend with respect to the PF concentration is observed (see Table S3 of Supporting Information). Compared to DU-PF-*x*, TU-PF-*x* hybrids present a higher ratio of silica centers per ethoxy monomer. This imparts rigidity to the overall network, which then preserves its structure even upon incorporation of sterically-hindered species, such as the PF chains. This supports our hypothesis of a more distorted and less organized structure for TU-PF-*x* compared to DU-PF-*x*, which is directed by the different degrees of branching on the Jeffamine precursors.

The powder X-ray diffraction patterns of both sets of samples present the characteristic features of ureasils, with a primary band between 19.9-20.7° and a shoulder at 11.8-12.5° (Figure S5, Supporting Information). The main peak is associated with localized order in the siliceous network,[35,45] with a structural unit distance, *d*, ranging between 4.4 ± 0.1 Å (calculated using Bragg's Law), while the shoulder is ascribed to in-plane ordering of the siliceous domains.[44] The coherence length calculated using the Scherrer equation is 10.3 ± 0.8 Å and is similar to values reported in literature for ureasils.[39-40]

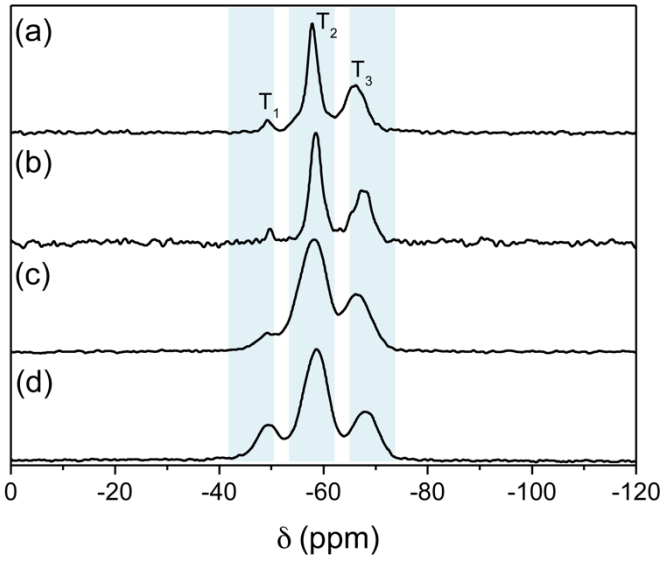


**Figure 4.** $^{29}$Si MAS-NMR spectra for (a) DU-PF-0.05, (b) DU-PF-0, (c) TU-PF-0.05 and (d) TU-PF-0.

The thermal stability of the samples is in good agreement with that previously observed in literature for di- and tri-ureasils,[30, 40] with a main decomposition event occurring at an onset temperature of ≈342-377 °C and ≈367-398 °C, for DU-PF-*x* and TU-PF-x, respectively (Figure S6, Supporting Information). The evaporation of residual solvent and of un-reacted ICPTES was also observed for some of the samples at temperatures between 70 and 190 °C.

**Evolution of the β-phase in PF-grafted ureasils.**

The optical properties of PFO are intrinsically linked to its morphology and, as such, can be used as a diagnostic probe of polymer conformation.[12] In dilute THF solution, the absorption and PL spectra of PFO-OH are characteristic of the α-phase, where each chain is individually dissolved and adopts a rigid rod-like conformation (Figure 5a).[46] The absorption and excitation spectra exhibit a single broad band centered at ~390 and ~380 nm, respectively. The corresponding PL spectrum displays the characteristic PF emission profile, featuring well-

resolved vibronic structure between 390-500 nm, ascribed to stretching modes associated with the polymer backbone.[4]

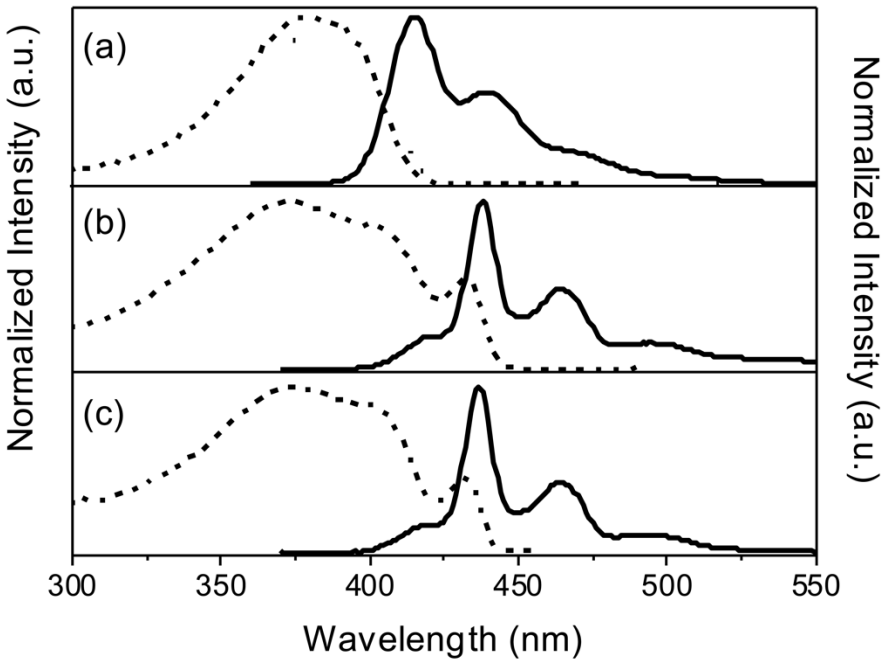


**Figure 5.** Absorption/ excitation (dotted line) and emission (solid line) spectra of (a) PFO-OH in THF solution ($10^{-6}$ mol × $dm^{-3}$, $\lambda_{ex}$ = 350 nm, $\lambda_{em}$ = 480 nm), (b) DU-PF-0.01 and (c) TU-PF-0.01 ($\lambda_{ex}$ = 360 nm, $\lambda_{em}$ = 500 nm).

Upon grafting of PFO-OH to the di-ureasil (Figure 5b) or tri-ureasil (Figure 5c), significant changes in the excitation and PL spectra are observed. A significant red-shift (*ca*. 20 nm) in the emission maximum is accompanied by the appearance of a new peak in the excitation spectra centered at 432 nm. These spectral changes are indicative of the formation of the β-phase, in which the PF chains undergo a conformational change guided by π-π interactions between their backbones leading to the formation of the more planar phase.[4, 12, 47] However, the excitation and emission spectra still display optical contributions from the α-phase, confirming co-existence of the two phases. As the PFO-OH concentration is increased, the peaks in the PL spectra became broader, the wavelength of the 0-0 vibronic transition red-shifts and the relative

intensities of the maxima change (Figure S7 and Figure S8, Supporting Information). For the DU-PF-*x* series, the 0-0 transition of the beta phase red-shifts from 438 to 441 nm to 444 nm upon increasing the concentration of PF from 0.01 to 0.05 to 0.1 %w/w. The same transition for the corresponding TU-PF-*x* series, red-shifts from 437 nm to 439 nm when the concentration of PF increases from 0.01 to 0.05% w/w, but remains constant thereafter.

As previously shown for poly[9,9-bis(2-ethylhexyl)-fluorene] and polyethylene blends, this optical behavior is characteristic of self-absorption, which suggests that segregated microdomains form, in which the PF chains are close to each other.[48] Notably, neither DU-PF-*x* or TU-PF-*x* samples exhibit the excitation-energy dependent emission properties associated with ureasils suggesting that electronic communication between the two components is negligible.[49] This is in direct contrast to the behavior observed for physically-immobilized conjugated polymer-ureasil composites, in which excitonic migration results in enhanced photoluminescence quantum yields[30] or tunable emission colors.[39]

The photoluminescence and excitation spectra of DU-PF-0.01 were followed as a function of the gelation time to evaluate the temporal evolution of the β-phase within the ureasil (Figure 6a,b). In the initial sol ($t = 0$), the PF chains are in the α-phase conformation. Upon addition of the gelation reagents ($H_3O^+$, EtOH), the solution becomes increasingly viscous as the sol-gel transition proceeds. The emission band associated with the α-phase decreases progressively in intensity from 0-28 h, after which time the optical fingerprint of the β-phase emerges. This is confirmed by the concomitant increase in the intensity of the characteristic peak of the β-phase centered at 435 nm in the excitation spectrum. Both peaks increase in intensity with time, reaching a maximum as the condensation reaction reaches completion ($t$ = 143 h). Similar behavior was reported for the gelation of PFO in the poor solvent methylcyclohexane (concentration of 1.0 wt%) at 20 °C.[50] The evolution of the β-phase over time is consistent is

consistent with the transition from a fluid to a more confined environment for PFO-OH as the sol-gel transitions proceeds, which promotes π-π stacking of the conjugated backbone.

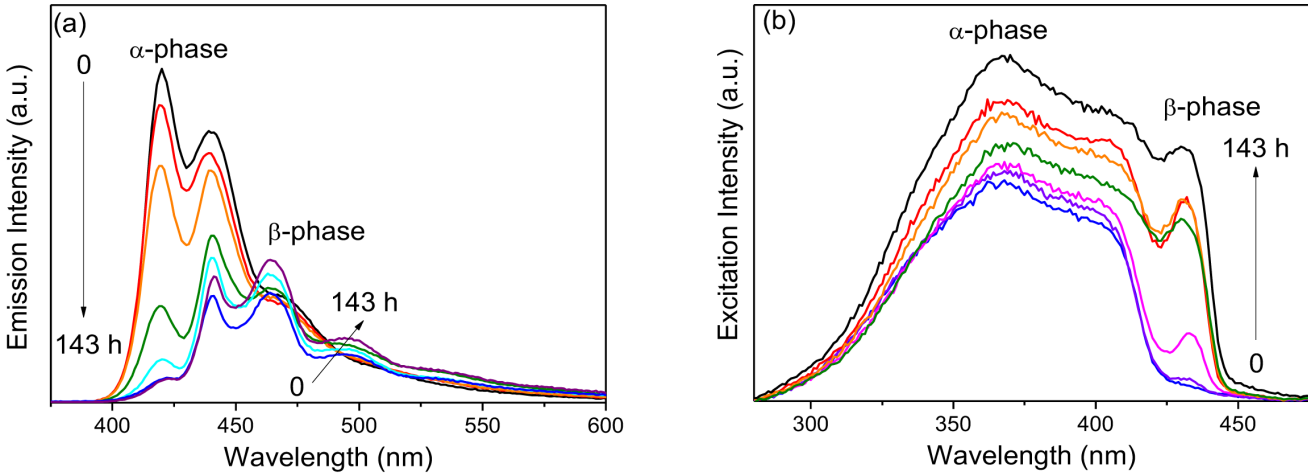


**Figure 6.** (a) Emission ($\lambda_{ex}$ = 360 nm) and (b) excitation ($\lambda_{em}$ = 500 nm) spectra of DU-PF-0.01 recorded as a function of time after initiation of the sol-gel reaction (t = 0 → 143 h).

To quantify the contribution of the β-phase to the optical properties of PF-ureasils, multi-peak Gaussian deconvolution was performed on the excitation spectrum of DU-PF-0.01 (Figure 7a). Five distinct components could be isolated, which is reasonable since the final excitation spectrum of each PF-ureasil arises from contributions from PFO-OH chains adopting either the α- or β-phase, and the ureasil network. The components were assigned as follows: (i) the isolated β-phase peak (~2.9 eV); (ii) the 0-0 electronic transition of the α-phase at ~3.1 eV (see Gaussian-fits for PFO-OH in the α-phase in Figure S9, Supporting Information); (iii) and (iv) are overlapping contributions from the $\nu_1$ vibronic transition of the α-phase (~3.3 eV) and the ureasil emission (~2.9-3.4 eV) and (v) higher order vibronic bands (~4.2 eV) associated with the PF. We note that the origin of the photoluminescence properties of ureasil-type materials have been widely studied and comprises two components ascribed to electron-hole recombination occurring in the siliceous nanodomains (~3.2-3.7 eV, so-called *purple* component) and photoinduced proton transfer occurring in the NH groups of the urea linkages

(~2.7-3.5 eV, so-called *blue* component), respectively.[45, 51] Similar results were obtained for samples in the entire DU-PF-*x* and TU-PF-*x* series (Figure S10 in Supporting Information).

For pure PF systems, the contribution of the β-phase is usually quantified by subtraction of the absorption spectrum of the PF mixed-phase solution/thin film from that of the corresponding sample adopting a pure α-phase.[16, 52] In our case, the significant overlap between the α-phase and ureasil excitation spectra prevents the isolation of the individual PFO-OH components. However, as previously shown by Knaapila *et al.*,[53] Gaussian fits can be used to successfully isolate the distinct peak corresponding to the β-phase, allowing us to quantify its relative contribution to the global excitation spectrum.

For both DU-PF-*x* and TU-PF-*x* hybrids, the β-phase contribution increases gradually when the PFO-OH concentration is initially increased from to 7.5 and 5.1% respectively (Figure 7b), before dropping slightly to 4.1% and 4.6%, at the highest PF concentration. Figure 7b also compares the corresponding photoluminescence quantum yields ($\Phi_{PL}$) as a function of PF concentration. DU-PF-0 and TU-PF-0 exhibit a $\Phi_{PL}$ of 1.5% (±0.2%) and 3.0 (±0.1%), respectively, which are in reasonable agreement with values reported in the literature for pure di- and tri-ureasils.[35, 43] At high PF concentrations, the decrease in the intensity of the 0-0 vibronic band in the photoluminescence spectra indicates that self-absorption significantly affects the emission properties of these samples.[27] The $\Phi_{PL}$ values obtained for DU-PF-*x* and TU-PF-*x* before and after correction for self-absorption[54] are also shown in Table S4. The incorporation of PFO-OH results in a drastic increase in $\Phi_{PL}$, ranging from 56.8-66.4% and 80.2-82.6% for DU-PF-*x* and TU-PF-*x*, respectively, after correction. Notably, the $\Phi_{PL}$ for the TU-PF series is in excellent agreement with that obtained for PFO-OH in a THF solution ($\Phi_{PL}$ = 85.3 ± 2.2%). For conjugated polymers in general, transfer to the solid state often leads to a decrease in the $\Phi_{PL}$ of the final material.[55] Our results suggest that at any of the studied concentrations, inclusion into the t-U(403) matrix results in a homogeneous dispersion of the

PF chains within the tri-ureasil host, thus inhibiting aggregation-induced quenching. For the DU-PF-*x* series however, the lowest $\Phi_{PL}$ (56.8 ± 1.2%) is obtained for DU-PF-0.05, which also displays the highest percentage of β-phase (7.46%). It has previously been shown that for PF films that a high β-phase contribution can lower the PLQY due to the formation of chemical defects in the polymer structure that are not related to the chain conformation of the polymer.[56]

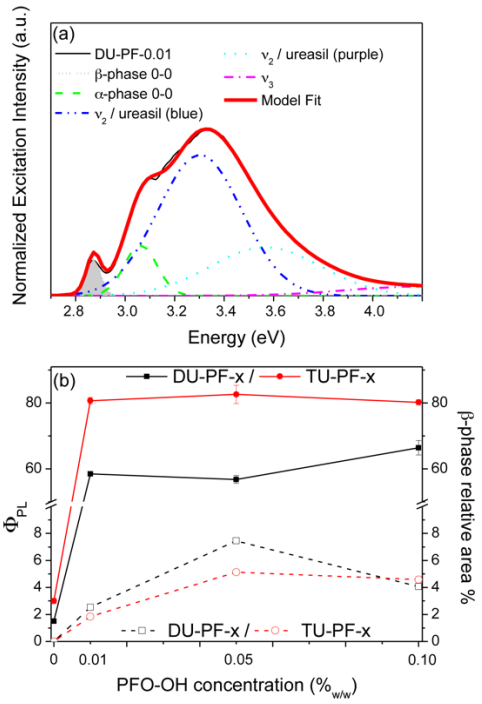


**Figure 7.** (a) Area-normalized excitation spectrum of DU-PF-0.01 ($\lambda_{em}$ = 480 nm) and corresponding Gaussian fits of the spectral components associated with the vibronic modes of PFO-OH, where $\nu_n$ refers to the vibrational mode, n, and the blue and purple components of the ureasil. The shaded area corresponds to the pure β phase component. (b) % β-phase contribution (open symbols) and photoluminescence quantum yields (solid symbols) as a function of the PFO-OH wt% for the DU-PF-*x* and TU-PF-*x* series. The solid and dashed lines serve only to guide the eye.

The global results suggest that the branching of the ureasil network has a significant impact on the packing and localization of the covalently-grafted PF chains within the siliceous

backbone, which controls the extent of β phase formation and the resultant optical properties. Figure 8 presents a schematic representation of the proposed packing arrangement of the polymer chains in DU-PF-*x* and TU-PF-*x* hybrids. For the TU-PF-*x* series, structural analysis showed that there are no major differences in the hydrogen bonding arrangements for pure and doped tri-ureasils at any of the concentrations studied, suggesting that the PF chains must adapt their conformation to that of the ureasil framework. As the concentration of PFO-OH is increased, its tendency to aggregate is hindered by the rigidity of the siliceous backbone, which not only imparts a certain level of structural control over the PFO-OH chains, but also prevents it from hosting more than a fixed volume of PF within each domain due to steric hindrance. This also restricts the number of covalent interactions between the PF-PTES precursor and the tri-ureasil. As such, we propose that the PF chains will tend to populate all vacant cavities in the hybrid, yielding a homogeneous distribution of smaller occupied domains, rather than forming larger isolated pockets. This accounts for the comparable percentage of β-phase formed (~5%) and similar degrees of condensation of the siliceous network for TU-PF-0.05 and TU-PF-0.1. Conversely, for DU-PF-*x*, FTIR measurements showed that the incorporation of PFO-OH slightly favors urea-urea ordered bonding interactions, suggesting a more packed structure. We propose that the linear branching of Jeffamine ED-600 facilitates better packing of the PFO-OH chains, providing more opportunities for covalent grafting of the PF-PTES precursor to the di-ureasil via the siliceous backbone. This is further supported by the red-shift in the wavelength of the 0-0 vibronic transition associated with the β-phase in the emission spectrum, which is larger and exhibits a more significant concentration dependence for the DU-PF-*x* series.

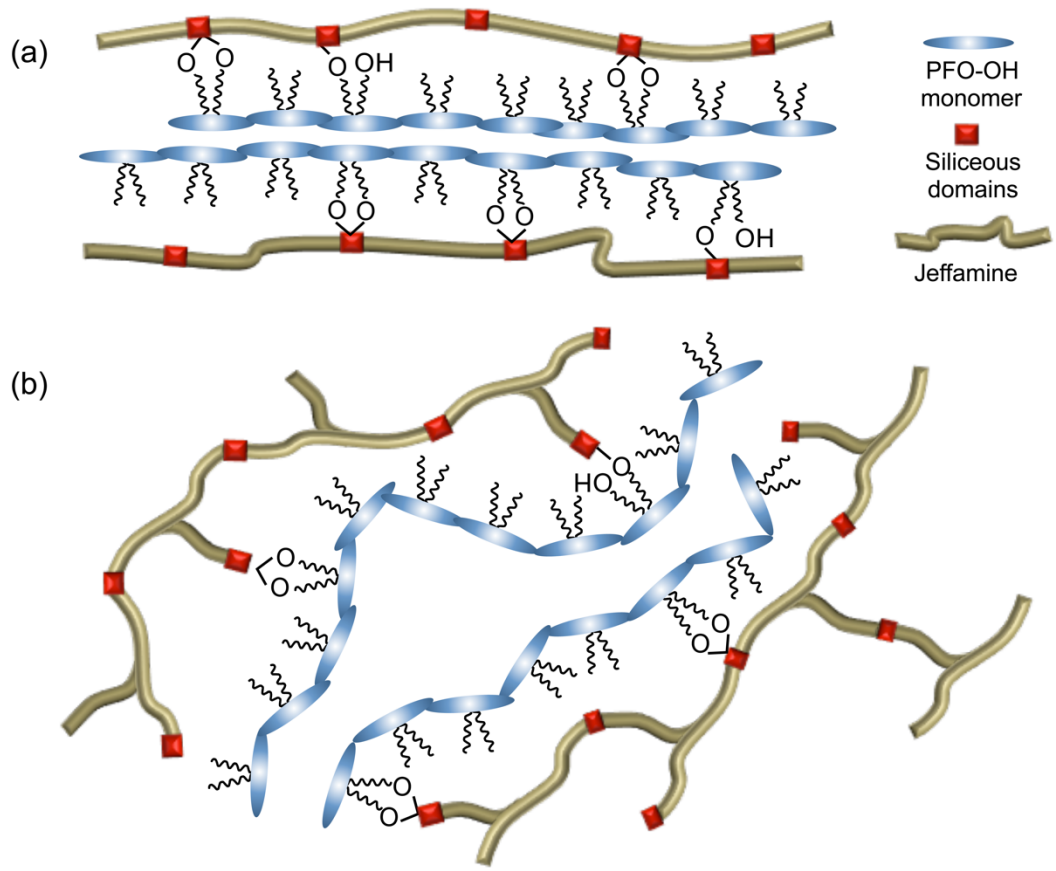


**Figure 8.** Schematic representation of the proposed structure for the stacking of PFO-OH in (a) DU-PF-x and (b) TU-PF-x (not to scale).

## CONCLUSIONS

Formation of the poly(fluorene) β-phase can be promoted through covalent-grafting of the hydroxyl-functionalized PFO-OH to di- and tri-ureasil organic-inorganic hybrids. Covalent grating of the PFO-OH chains to the siloxane backbone of the ureasil precursor was confirmed using a combination of spectroscopic and structural analyses, and to the best of our knowledge these materials are the first examples of macroscopic Class II organic-inorganic hybrids incorporating conjugated polymers. Whilst grafting occurs at the inorganic domains, the degree of branching of the PEO/PPO organic backbone (*i.e.* the Jeffamine) determines the extent of packing of the PFO-OH within the ureasil, and thus the conformation of the polymer chains. FTIR studies revealed that while fairly strong hydrogen bonding interactions dominate in the

linear PF-di-ureasils, the PF-tri-ureasils exhibit a more open and distorted structure, which restricts the efficacy of packing and reduces the number of covalent interactions. This was also confirmed by the degree of condensation determined from $^{29}$Si MAS-NMR studies, which was generally higher for di-ureasils than tri-ureasils. The role of steric confinement was further evidenced in the temporal evolution of the optical fingerprint of the β-phase as the samples undergo the sol-gel transition. PL and UV/Vis absorption studies revealed that in a good solvent (THF), PFO-OH adopts the α-phase. In contrast, upon incorporation in the ureasil matrix, the PF chains undergo a conformational change directed by the branching of the ureasil framework, which promotes the formation of the β-phase and leads to distinct changes in the PL emission and excitation profiles of the samples. Reports of β-phase formation in multicomponent systems are extremely limited[26, 28] and the system investigated here has provided key insight on the role of spatial confinement, coupled with physical interactions, on the formation mechanism. Moreover, the observation of the β-phase in the TU-PF-*x* series, where the network structure is more open and where interchain interactions are expected to be less important, provides experimental support for the possibility of β-phase formation on isolated chains, as suggested by the single molecule spectroscopy experiments performed by Lupton *et al*.[57]

Notably, the ability to control and tune the extent of the β-phase contribution by changing the degree of branching of the organic backbone of the host has important implications the rational design of high-performance hybrid light-emitting diodes and organic lasers, where the β-phase may be desired.[23, 58]

## ASSOCIATED CONTENT

**Supporting Information**.

TGA for PFO-OH, ICPTES and PF-PTES, FTIR for ICPTES, Jeffamine ED-600, Jeffamine

T-403, d-UPTES, t-UPTES, DU-PF-*x* and TU-PF-x, PXRD, $^{13}$C and $^{29}$Si MAS-NMR, supporting PL measurements (emission and excitation spectra, Gaussian deconvolution, PL quantum yields). The following files are available free of charge. Meazzinietal_2017_ESI.pdf

AUTHOR INFORMATION

**Corresponding Author**

*E-mail: raevans@tcd.ie

**Present Addresses**

†Department of Materials Science and Metallurgy, University of Cambridge, 27 Charles Babbage Road, Cambridge CB3 0FS, U.K. Email: rce26@cam.ac.uk

**Author Contributions**

The manuscript was written through contributions of all authors. All authors have given approval to the final version of the manuscript.

**Funding Sources**

This work was supported by the Science Foundation Ireland under Grant No. 12/IP/1608.

**ACKNOWLEDGMENTS**

The authors thank Dr Niamh Willis-Fox for assistance with initial data collection. Solid-state NMR spectra were obtained at the EPSRC UK National Solid-state NMR Service at Durham. MLT thanks the EPSRC Centre for Manufacturing in Large Area Electronics (EP/K03099X/1) and the Knowledge Centre for Materials Chemistry for financial support.

**REFERENCES**

(1) Cook, J. H.; Santos, J.; Li, H.; Al-Attar, H. A.; Bryce, M. R.; Monkman, A. P., Efficient Deep Blue Fluorescent Polymer Light-Emitting Diodes (PLEDs). *J. Mater. Chem. C* **2014**, *2*, 5587-5592.
(2) Schelkle, K. M.; Bender, M.; Jeltsch, K.; Buckup, T.; Müllen, K.; Hamburger, M.; Bunz, U. H. F., Light-Induced Solubility Modulation of Polyfluorene To Enhance the Performance of OLEDs. *Angew. Chem. Int. Ed.* **2015**, *54*, 14545-14548.
(3) Luo, J.; Zhou, Y.; Niu, Z.-Q.; Zhou, Q.-F.; Ma, Y.; Pei, J., Three-Dimensional Architectures for Highly Stable Pure Blue Emission. *J. Am. Chem. Soc.* **2007**, *129*, 11314-11315.
(4) Scherf, U.; List, E. J. W., Semiconducting Polyfluorenes—Towards Reliable Structure–Property Relationships. *Adv. Mater.* **2002**, *14*, 477-487.
(5) Zhong, C.; Duan, C.; Huang, F.; Wu, H.; Cao, Y., Materials and Devices toward Fully Solution Processable Organic Light-Emitting Diodes. *Chem. Mater.* **2011**, *23*, 326-340.
(6) Lv, F.; Qiu, T.; Liu, L.; Ying, J.; Wang, S., Recent Advances in Conjugated Polymer Materials for Disease Diagnosis. *Small* **2016**, *12*, 696-705.
(7) Cingil, H. E.; Storm, I. M.; Yorulmaz, Y.; te Brake, D. W.; de Vries, R.; Cohen Stuart, M. A.; Sprakel, J., Monitoring Protein Capsid Assembly with a Conjugated Polymer Strain Sensor. *J. Am. Chem. Soc.* **2015**, *137*, 9800-9803.
(8) Shi, H.; Ma, X.; Zhao, Q.; Liu, B.; Qu, Q.; An, Z.; Zhao, Y.; Huang, W., Ultrasmall Phosphorescent Polymer Dots for Ratiometric Oxygen Sensing and Photodynamic Cancer Therapy. *Adv. Funct. Mater.* **2014**, *24*, 4823-4830.
(9) Shi, H.; Sun, H.; Yang, H.; Liu, S.; Jenkins, G.; Feng, W.; Li, F.; Zhao, Q.; Liu, B.; Huang, W., Cationic Polyfluorenes with Phosphorescent Iridium(III) Complexes for Time-Resolved Luminescent Biosensing and Fluorescence Lifetime Imaging. *Adv. Funct. Mater.* **2013**, *23*, 3268-3276.
(10) Zhu, C.; Liu, L.; Yang, Q.; Lv, F.; Wang, S., Water-Soluble Conjugated Polymers for Imaging, Diagnosis, and Therapy. *Chem. Rev.* **2012**, *112*, 4687-4735.
(11) Almeida, C. S.; Herrmann, I. K.; Howes, P. D.; Stevens, M. M., Tailoring Cellular Uptake of Conjugated Polymer Nanoparticles Using Modular Amphiphilic Peptide Capping Ligands. *Chem. Mater.* **2015**, *27*, 6879-6889.
(12) Knaapila, M.; Monkman, A. P., Methods for Controlling Structure and Photophysical Properties in Polyfluorene Solutions and Gels. *Adv. Mater.* **2013**, *25*, 1090-1108.

(13) Bright, D. W.; Dias, F. B.; Galbrecht, F.; Scherf, U.; Monkman, A. P., The Influence of Alkyl-Chain Length on Beta-Phase Formation in Polyfluorenes. *Adv. Funct. Mater.* **2009**, *19*, 67-73.
(14) Lin, Z.-Q.; Shi, N.-E.; Li, Y.-B.; Qiu, D.; Zhang, L.; Lin, J.-Y.; Zhao, J.-F.; Wang, C.; Xie, L.-H.; Huang, W., Preparation and Characterization of Polyfluorene-Based Supramolecular π-Conjugated Polymer Gels. *J. Phys. Chem. C* **2011**, *115*, 4418-4424.
(15) Huang, L.; Zhang, L.; Huang, X.; Li, T.; Liu, B.; Lu, D., Study of the α-Conformation of the Conjugated Polymer Poly(9,9-dioctylfluorene) in Dilute Solution. *J. Phys. Chem. B* **2014**, *118*, 791-799.
(16) Cadby, A.; Lane, P.; Mellor, H.; Martin, S.; Grell, M.; Giebeler, C.; Bradley, D.; Wohlgenannt, M.; An, C.; Vardeny, Z., Film Morphology and Photophysics of Polyfluorene. *Phys. Rev. B* **2000**, *62*, 15604.
(17) Knaapila, M.; Torkkeli, M.; Galbrecht, F.; Scherf, U., Crystalline and Noncrystalline Forms of Poly(9,9-diheptylfluorene). *Macromolecules* **2013**, *46*, 836-843.
(18) Evans, R. C.; Macedo, A. G.; Pradhan, S.; Scherf, U.; Carlos, L. D.; Burrows, H. D., Fluorene Based Conjugated Polyelectrolyte/Silica Nanocomposites: Charge-Mediated Phase Aggregation at the Organic–Inorganic Interface. *Adv. Mater.* **2010**, *22*, 3032-3037.
(19) Rothe, C.; Galbrecht, F.; Scherf, U.; Monkman, A., The β-Phase of Poly(9,9-dioctylfluorene) as a Potential System for Electrically Pumped Organic Lasing. *Adv. Mater.* **2006**, *18*, 2137-2140.
(20) Prins, P.; Grozema, F. C.; Schins, J. M.; Savenije, T. J.; Patil, S.; Scherf, U.; Siebbeles, L. D. A., Effect of Intermolecular Disorder on the Intrachain Charge Transport in Ladder-Type Poly(*p*-phenylenes). *Phys. Rev. B* **2006**, *73*, 045204.
(21) Chen, S. H.; Su, A. C.; Chen, S. A., Noncrystalline Phases in Poly(9,9-di-n-octyl-2,7-fluorene). *J. Phys. Chem. B* **2005**, *109*, 10067-10072.
(22) Bright, D. W.; Moss, K. C.; Kamtekar, K. T.; Bryce, M. R.; Monkman, A. P., The β Phase Formation Limit in Two Poly(9,9-di-n-octylfluorene) based Copolymers. *Macromol. Rapid Commun.* **2011**, *32*, 983-987.
(23) Kuehne, A. J. C.; Kaiser, M.; Mackintosh, A. R.; Wallikewitz, B. H.; Hertel, D.; Pethrick, R. A.; Meerholz, K., Sub-Micrometer Patterning of Amorphous- and β-Phase in a Crosslinkable Poly(9,9-dioctylfluorene): Dual-Wavelength Lasing from a Mixed-Morphology Device. *Adv. Funct. Mater.* **2011**, *21*, 2564-2570.

(24) Banach, M. J.; Friend, R. H.; Sirringhaus, H., Influence of the Casting Solvent on the Thermotropic Alignment of Thin Liquid Crystalline Polyfluorene Copolymer Films. *Macromolecules* **2004**, *37*, 6079-6085.
(25) de Francisco, R.; Hoyos, M.; García, N.; Tiemblo, P., Superhydrophobic and Highly Luminescent Polyfluorene/Silica Hybrid Coatings Deposited onto Glass and Cellulose-Based Substrates. *Langmuir* **2015**, *31*, 3718-3726.
(26) Evans, R. C.; Marr, P. C., Chain Confinement Promotes β-Phase Formation in Polyfluorene-Based Photoluminescent Ionogels. *Chem. Commun.* **2012**, *48*, 3742-3744.
(27) Marr, P. C.; McBride, K.; Evans, R. C., Sugar-derived Organogels as Templates for Structured, Photoluminescent Conjugated Polymer-Inorganic Hybrid Materials. *Chem. Commun.* **2013**, *49*, 6155-6157.
(28) Behrendt, J. M.; Foster, A. B.; McCairn, M. C.; Willcock, H.; O'Reilly, R. K.; Turner, M. L., Hybrid Inorganic-Organic Composite Nanoparticles from Crosslinkable Polyfluorenes. *J. Mater. Chem. C* **2013**, *1*, 3297-3304.
(29) Morisaki, Y.; Tsuji, Y.; Chujo, Y., Versatile hybridization of conjugated polymers with silica. *J. Mater. Chem.* **2011**, *21*, 14402-14405.
(30) Willis-Fox, N.; Marques, A.-T.; Arlt, J.; Scherf, U.; Carlos, L. D.; Burrows, H. D.; Evans, R. C., Synergistic Photoluminescence Enhancement in Conjugated Polymer-Di-Ureasil Organic-Inorganic Composites. *Chem. Sci.* **2015**, *6*, 7227-7237.
(31) Ueda, K.; Tanaka, K.; Chujo, Y., Remarkably high miscibility of octa-substituted POSS with commodity conjugated polymers and molecular fillers for the improvement of homogeneities of polymer matrices. *Polym. J.* **2016**, *48*, 1133-1139.
(32) de Zea Bermudez, V.; Carlos, L. D.; Alcácer, L., Sol–Gel Derived Urea Cross-Linked Organically Modified Silicates. 1. Room Temperature Mid-Infrared Spectra. *Chem. Mater.* **1999**, *11*, 569-580.
(33) Carlos, L. D.; Ferreira, R. A. S.; de Zea Bermudez, V.; Ribeiro, S. J. L., Full-Color Phosphors from Amine-Functionalized Crosslinked Hybrids Lacking Metal Activator Ions. *Adv. Funct. Mater.* **2001**, *11*, 111-115.
(34) Correia, S. F. H.; de Zea Bermudez, V.; Ribeiro, S. J. L.; André, P. S.; Ferreira, R. A. S.; Carlos, L. D., Luminescent Solar Concentrators: Challenges for Lanthanide-Based Organic-Inorganic Hybrid Materials. *J. Mater. Chem. A* **2014**, *2*, 5580-5596.

(35) Lima, P. P.; Ferreira, R. A. S.; Júnior, S. A.; Malta, O. L.; Carlos, L. D., Terbium(III)-Containing Organic–Inorganic Hybrids Synthesized through Hydrochloric Acid Catalysis. *J. Photochem. Photobiol. A* **2009**, *201*, 214-221.
(36) Carlos, L. D.; Ferreira, R. A. S.; Orion, I.; de Zea Bermudez, V.; Rocha, J., Sol–gel Derived Nanocomposite Hybrids for Full Colour Displays. *J. Lumin.* **2000**, *87–89*, 702-705.
(37) Nolasco, M. M.; Vaz, P. M.; Freitas, V. T.; Lima, P. P.; André, P. S.; Ferreira, R. A. S.; Vaz, P. D.; Ribeiro-Claro, P.; Carlos, L. D., Engineering highly efficient Eu(iii)-Based Tri-Ureasil Hybrids Toward Luminescent Solar Concentrators. *J. Mater. Chem. A* **2013**, *1*, 7339-7350.
(38) Kaniyoor, A.; McKenna, B.; Comby, S.; Evans, R. C., Design and Response of High-Efficiency, Planar, Doped Luminescent Solar Concentrators Using Organic–Inorganic Di-Ureasil Waveguides. *Adv. Opt. Mater.* **2016**, *4*, 444-456.
(39) Willis-Fox, N.; Kraft, M.; Arlt, J.; Scherf, U.; Evans, R. C., Tunable White-Light Emission from Conjugated Polymer-Di-Ureasil Materials. *Adv. Funct. Mater.* **2016**, *26*, 532-542.
(40) Meazzini, I.; Willis-Fox, N.; Blayo, C.; Arlt, J.; Clément, S.; Evans, R. C., Targeted Design Leads to Tunable Photoluminescence from Perylene Dicarboxdiimide-Poly(oxyalkylene)/siloxane Hybrids for Luminescent Solar Concentrators. *J. Mater. Chem. C* **2016**, *4*, 4049-4059.
(41) de Zea Bermudez, V.; Ferreira, R. A. S.; Carlos, L. D.; Molina, C.; Dahmouche, K.; Ribeiro, S. J. L., Coordination of Eu3+ Ions in Siliceous Nanohybrids Containing Short Polyether Chains and Bridging Urea Cross-links. *J. Phys. Chem. B* **2001**, *105*, 3378-3386.
(42) Cui, Y.; Wang, M.; Chen, L.; Qian, G., Synthesis and Spectroscopic Characterization of an Alkoxysilane Dye Containing C. I. Disperse Red 1. *Dyes Pigm.* **2004**, *62*, 43-47.
(43) Freitas, V. T.; Lima, P. P.; Ferreira, R. A. S.; Pecoraro, E.; Fernandes, M.; de Zea Bermudez, V.; Carlos, L. D., Luminescent Urea Cross-Linked Tripodal Siloxane-Based Hybrids. *J. Sol-Gel Sci. Technol.* **2012**, *65*, 83-92.
(44) Fu, L.; Ferreira, R. A. S.; Silva, N. J. O.; Carlos, L. D.; de Zea Bermudez, V.; Rocha, J., Photoluminescence and Quantum Yields of Urea and Urethane Cross-Linked Nanohybrids Derived from Carboxylic Acid Solvolysis. *Chem. Mater.* **2004**, *16*, 1507-1516.
(45) Carlos, L. D.; de Zea Bermudez, V.; Ferreira, R. A. S.; Marques, L.; Assunção, M., Sol–Gel Derived Urea Cross-Linked Organically Modified Silicates. 2. Blue-Light Emission. *Chem. Mater.* **1999**, *11*, 581-588.

(46) Knaapila, M.; Garamus, V. M.; Dias, F. B.; Almásy, L.; Galbrecht, F.; Charas, A.; Morgado, J.; Burrows, H. D.; Scherf, U.; Monkman, A. P., Influence of Solvent Quality on the Self-Organization of Archetypical Hairy Rods−Branched and Linear Side Chain Polyfluorenes: Rodlike Chains versus "Beta-Sheets" in Solution. *Macromolecules* **2006**, *39*, 6505-6512.
(47) Grell, M.; Bradley, D. D. C.; Ungar, G.; Hill, J.; Whitehead, K. S., Interplay of Physical Structure and Photophysics for a Liquid Crystalline Polyfluorene. *Macromolecules* **1999**, *32*, 5810-5817.
(48) Knaapila, M.; Vaughan, H. L.; Hase, T. P. A.; Evans, R. C.; Stepanyan, R.; Torkkeli, M.; Burrows, H. D.; Scherf, U.; Monkman, A. P., Concentration Effect on the Oriented Microstructure in Tensile Drawn Polyfluorene–Polyethylene Blend. *Macromolecules* **2010**, *43*, 299-305.
(49) Ferreira, R. A. S.; Ferreira, A. L.; Carlos, L. D., Modeling of the Emission Red-shift in Organic–Inorganic Di-ureasil Hybrids. *J. Non-Cryst. Solids* **2006**, *352*, 1225-1229.
(50) Chen, C.-Y.; Chang, C.-S.; Huang, S.-W.; Chen, J.-H.; Chen, H.-L.; Su, C.-I.; Chen, S.-A., Phase-Separation-Induced Gelation of Poly(9,9-dioctylfluorene)/Methylcyclohexane Solution. *Macromolecules* **2010**, *43*, 4346-4354.
(51) Nobre, S. S.; Lima, P. P.; Mafra, L.; Ferreira, R. A. S.; Freire, R. O.; Fu, L.; Pischel, U.; de Zea Bermudez, V.; Malta, O. L.; Carlos, L. D., Energy Transfer and Emission Quantum Yields of Organic–Inorganic Hybrids Lacking Metal Activator Centers. *J. Phys. Chem. C* **2007**, *111*, 3275-3284.
(52) Shaw, P. E.; Ruseckas, A.; Peet, J.; Bazan, G. C.; Samuel, I. D. W., Exciton–Exciton Annihilation in Mixed-Phase Polyfluorene Films. *Adv. Funct. Mater.* **2010**, *20*, 155-161.
(53) Knaapila, M.; Bright, D. W.; Stepanyan, R.; Torkkeli, M.; Almásy, L.; Schweins, R.; Vainio, U.; Preis, E.; Galbrecht, F.; Scherf, U.; Monkman, A. P., Network Structure of Polyfluorene Sheets as a Function of Alkyl Side Chain Length. *Phys. Rev. E* **2011**, *83*, 051803.
(54) Ahn, T.-S.; Al-Kaysi, R. O.; Müller, A. M.; Wentz, K. M.; Bardeen, C. J., Self-Absorption Correction for Solid-State Photoluminescence Quantum Yields Obtained from Integrating Sphere Measurements. *Rev. Sci. Instrum.* **2007**, *78*, 086105.
(55) Tan, C.; Atas, E.; Müller, J. G.; Pinto, M. R.; Kleiman, V. D.; Schanze, K. S., Amplified Quenching of a Conjugated Polyelectrolyte by Cyanine Dyes. *J. Am. Chem. Soc.* **2004**, *126*, 13685-13694.

(56) Bansal, A. K.; Ruseckas, A.; Shaw, P. E.; Samuel, I. D. W., Fluorescence Quenchers in Mixed Phase Polyfluorene Films. *J. Phys. Chem. C* **2010**, *114*, 17864-17867.
(57) Da Como, E.; Borys, N. J.; Strohriegl, P.; Walter, M. J.; Lupton, J. M., Formation of a Defect-Free π-Electron System in Single β-Phase Polyfluorene Chains. *J. Am. Chem. Soc.* **2011**, *133*, 3690-3692.
(58) Yang, Y.; Turnbull, G. A.; Samuel, I. D. W., Sensitive Explosive Vapor Detection with Polyfluorene Lasers. *Adv. Funct. Mater.* **2010**, *20*, 2093-2097.

**Table of Contents:**